UNIVERSIDAD DE CHILE
FACULTAD DE CIENCIAS FÍSICAS Y MATEMÁTICAS
DEPARTAMENTO DE INGENIERÍA CIVIL

ANÁLISIS EXPERIMENTAL Y NUMÉRICO DE ESTANQUES DE ALMACENAMIENTO DE COMBUSTIBLE CON DIVERSAS TECNOLOGÍAS DE VENTILACIÓN SOMETIDOS A DEFLAGRACIONES INTERNAS

MEMORIA PARA OPTAR AL TÍTULO DE INGENIERO CIVIL

LUIS RAMÓN CÁRCAMO DEL RÍO

PROFESOR GUÍA:

FRANCISCO JAVIER HERNÁNDEZ PRADO

MIEMBROS DE LA COMISIÓN:

FELIPE OCHOA CORNEJO

RICARDO HERRERA MARDONES

SANTIAGO DE CHILE

2023

ANÁLISIS EXPERIMENTAL Y NUMÉRICO DE ESTANQUES DE ALMACENAMIENTO DE COMBUSTIBLE CON DIVERSAS TECNOLOGÍAS DE VENTILACIÓN SOMETIDOS A DEFLAGRACIONES INTERNAS.

Se realizó un estudio experimental y numérico en estanques de almacenamiento de combustible a pequeña escala sometidos a deflagraciones causadas por explosiones de mezclas de metano-aire. Se investigaron tres tecnologías para una despresurización eficiente a través del techo del estanque. La ventilación rápida a través del techo permite mitigar la sobrepresión generada dentro de los estanques, evitando otros daños catastróficos, como la falla en la unión entre el manto y el fondo. En primer lugar, se examinó un estanque a pequeña escala con un techo frangible; su activación se desencadenó debido a la falla local de las soldaduras alrededor del perímetro del techo en la unión entre la placa del techo y el manto. El segundo estanque considera una estrategia de ventilación secuencial lograda mediante una puerta con bisagras ubicada en la interfaz entre el techo y manto, seguida de la falla del techo a través de las soldaduras perimetrales. Esta estrategia de ventilación secuencial se adapta a la intensidad de la explosión, donde las explosiones de baja y mediana intensidad pueden mitigarse utilizando la pequeña abertura, evitando que todo el techo se desprenda. Como resultado, la operación puede recuperarse rápidamente volviendo a cerrar la pequeña abertura. En el caso de explosiones de gas devastadoras, la apertura de la abertura desencadena una activación anticipada del techo frangible y permite controlar la dirección en la que se abre el techo. Por último, se estudió un estanque con salidas de explosión comerciales como alternativa a los techos frangibles tradicionales, que pueden emplearse en estanques existentes sin un techo frangible. Se realizaron simulaciones estáticas y dinámicas en LS-DYNA para validar y comparar los resultados experimentales de todos los estanques de almacenamiento de combustible analizados. Las simulaciones revelaron que el colapso plástico del anillo de compresión puede retrasarse si ocurre una sobrepresión rápida. La alta ductilidad del acero puede retrasar la falla plástica, lo que significa que la presión puede superar significativamente la presión que desencadena el colapso plástico del anillo de compresión cuando se asume que la presión interna es estática. Además, la falla de la unión entre el techo y el manto puede atribuirse a la falla frágil de sus soldaduras, que parece explicarse por la deformación plástica local asociada con la base de la placa del techo. Como resultado, se sugiere emplear un criterio de falla de soldadura para evaluar la presión de activación del techo frangible de los estanques de almacenamiento de combustible sometidos a deflagraciones internas de gas.

EXPERIMENTAL AND NUMERICAL ANALYSIS OF FUEL STORAGE TANKS WITH VARIED VENTING TECHNOLOGIES SUBJECTED TO INTERNAL DEFLAGRATIONS

Francisco Hernandez[1], Luis Carcamo[2], Hong Hao[3], Xihong Zhang[3], Jingde Li[3]

[1] Facultad de Ingeniería y Ciencias Aplicadas, Universidad de los Andes, Monseñor Álvaro del Portillo Nº12.455, Las Condes, Santiago, Chile

[2] Department of Civil Engineering, University of Chile, Av. Blanco Encalada 2002, Santiago, Chile

[3] Centre for Infrastructural Monitoring and Protection, School of Civil and Mechanical Engineering, Curtin University, WA 6102, Australia

ABSTRACT

An experimental and numerical study was conducted on small-scale fuel storage tanks subjected to deflagrations caused by methane-air mixtures' explosions. Three technologies were investigated for efficient depressurization through the tank's roof. Rapid ventilation through the roof allows for mitigating the overpressure generated inside the tanks, preventing other catastrophic damage, such as shell-to-bottom joint failure. First, a small-scale tank with a frangible roof was examined; its activation was triggered due to the local failure of stitch welds allocated around the roof perimeter at the junction between the roof plate and the top angle. The second tank considers a sequential ventilation strategy achieved using a hinged door positioned at the interface between the roof and the top angle, followed by the roof failure through perimeter stitch welds. This sequential ventilation strategy adapts to the explosion intensity, where low- and medium-intensity explosions can be mitigated using the small vent, preventing the entire roof from detaching. As a result, the operation can be rapidly recovered by reclosing the small vent. In the case of devastating gas explosions, the vent's opening triggers an earlier activation of the frangible roof and allows control of the direction where the roof is opened. Lastly, a tank with commercial explosion vents was studied as an alternative to traditional frangible roofs, that can be employed for existing tanks without a frangible roof. Static and dynamic simulations in LS-DYNA were performed to validate and compare the experimental results for all the analyzed fuel storage tanks. Simulations revealed that the plastic collapse of the compression ring can be delayed if a fast overpressure occurs. The steel's high ductility can delay the plastic failure, meaning that the pressure can significantly exceed the pressure that triggers the compression ring's plastic collapse when the internal pressure is assumed to be static. Furthermore, the failure of the roof-to-shell junction can be attributed to the brittle failure of its welds, which seems to be explained by the local plastic strain associated with the roof plate metal base. As a result, it is suggested to employ a weld failure criterion to evaluate the frangible roof activation pressure of fuel storage tanks subjected to internal gas deflagrations.

AGRADECIMIENTOS

Mis más sinceros agradecimientos a Luis y María Jesús, mis queridos formadores, ejemplos de vida y amados padres. A lo largo de mi formación académica, han sido mi pilar fundamental, brindándome su amor y apoyo incondicional, sacrificado mucho para no dejar de creer en mí y en mis capacidades. También quiero extender este agradecimiento a mi hermano menor, Pedro, a quien quiero y amo profundamente. Si bien él no sabe, accidentalmente, me ha motivado a nunca dejar de ser un hermano mayor, del cual pueda orgullecer se y que siempre esté a la altura y expectativas de un modelo a seguir.

Un agradecimiento especial va para las chicas de mi grupo de Topografía: Paula, Pilar y Valentina. No solo fueron compañeras de trabajo en esa instancia, sino que se convirtieron en amigas y compañeras en muchas otras ocasiones, especialmente en tiempos de pandemia, cuando formar grupos de estudio resultó complicado. Aprecio profundamente su paciencia y comprensión, ya que en ocasiones fui un compañero de grupo poco comprometido. También deseo extender este agradecimiento a los grandes amigos que hice en la universidad: los de Hff, los Lindos, Chauto, el Waton entre otros. La universidad no solo es un lugar para estudiar, y junto a ustedes pude disfrutar mucho durante estos años.

Quiero expresar mi gratitud hacia todos los académicos que contribuyeron a mi crecimiento académico y profesional. En primer lugar, a los profesores Juan Felipe Beltrán y Ricardo Herrera, quienes confiaron en mí para formar parte de su equipo docente en innumerables ocasiones. Participar en cuerpos docentes dentro de la universidad fue una experiencia de gran valor formativo que me motivó y me hizo aprender mucho. Continuando en esta línea, agradezco a mi profesor guía, Francisco Hernández, quien no solo fue el docente que me inspiró a elegir mi especialidad cuando cursé mi primer ramo de ingeniería civil, sino que también confió en mí como profesor auxiliar en sus cursos. Esto fomentó mi pasión por la docencia, donde espero haber aportado lo mejor de mí al desarrollo académico de las futuras generaciones de ingenieros civiles de nuestra universidad.

Por último, deseo agradecer a la facultad y su área de relaciones internacionales. A través de un programa de movilidad estudiantil, ampliaron mi horizonte y perspectiva, tanto dentro como fuera de nuestro país. Esta experiencia fue una de las mejores que he tenido en mi vida y es el motivo, por el cual, decidí continuar mi aventura académica y profesional fuera de Chile.

Table of Content

1. Introduction

Fuel Storage (FS) tanks are widely used in the petroleum and chemical industries. These tanks typically feature a vertical, cylindrical, aboveground shell with a conical roof and a flat (or slightly conical) bottom. The roof plate is typically supported by rafters, which are consequently supported by the tank's shell and over a central column allocated at the center of the tank. The roof plate is not attached to the rafters but rests on them. During tank filling and emptying, the vapor above the liquid surface inside the tank may fall within its flammability limits. If this flammable vapor is accidentally ignited, a catastrophic loss of the tank integrity could occur due to a fast over pressurization (in a few milliseconds) generated by an internal gas explosion. In case the tank's shell-to-bottom joint fails, the stored fuel will be spilled into the surroundings [1]. As a result, the leaked fuel can lead to secondary external explosions and fires, damaging neighboring tanks and structures. To address this risk, current practices focus on providing a weak roof-to-shell junction that fails deliberately to prevent the FS tank collapse and avoid the failure of its shell-to-bottom joint. In other words, a frangible roof-to-shell joint should ensure massive ventilation, allowing reducing internal blast overpressure (slightly higher than the roof activation pressure), minimizing the probability of significant damage, and keep their storage capability.

The design rules of FS tanks and their frangible roofs are standardized by the American Petroleum Institute [2] and the European Committee for Standardization [3]. API 650 [2] states that a frangible roof is provided if "the roof-to-shell joint will fail prior to the shell-to-bottom joint in the event of excessive internal pressure". Consequently, API 650 establishes certain specifications that a frangible roof should comply such as: i) the tank shall have a diameter bigger than 15.25 m, ii) the roof slope should be smaller than 1/6, iii) the roof should be welded to the top angle using a continuous fillet weld that does not exceed 5 mm, iv) the roof plate should not be attached to rafters, v) the roof-to-top-angle compression ring is constrained to certain listed geometries and the cross-sectional area should be smaller than the pressure that equal the roof plates weight. In case the internal pressure exceeds the weight of the roof plates, the design pressure [2] that shall be utilized for designing anchorages, shell-to-bottom joints, foundations, nozzles, manholes, and shells corresponding to the pressure (with a safety factor of 1.6 [4]) that causes the plastic collapse of the compression ring, i.e., the yielding of the roof-to-shell junction.

FS tanks are not pictured as pressure vessels and their normal service internal overpressures are limited to less than 18 kPa [2] or 50 kPa [3] (and 100 kPa [5]). In other words, ordinary vent devices [2,3,5] are commonly included to ensure that the internal pressure remains close to atmospheric pressure under operating conditions (emptying, filling, temperature fluctuations, and external fires); however, conventional venting devices may not cope with the sudden and high rising pressure rate required by an internal gas explosion, implying that a frangible roof should be provided to provide the extra ventilation required to keep the integrity of the FS tank infrastructure.

Over the past 40 years, FS tanks with reduced slope cone roofs have been successful in most cases (particularly for tanks with diameters exceeding 12.5 meters [4]). However, evidence from various sources in the literature demonstrates that gas explosions are frequent and can cause devasting consequences on FS tanks worldwide [6–9]. Particularly, FS tanks with dome roofs, small-diameter tanks or with strong welds at the roof-to-shell connection have been especially susceptible to such failures [1,10]. There have been instances where failure occurred at the shell-to-bottom connection, causing tanks to be launched into the air and resulting in the dispersion of fuel, leading to severe fires and potential damage to nearby tanks. Additionally, accidents have occurred due to explosions in tanks containing a low fuel level, resulting in shell rupture. Therefore, it is extremely important that all actions should be taken during the tank design, the construction, the operation, and the maintenance to ensure, as far as possible, that the preferential failure occurs through the roof-to-shell joint.

Taking this into account, Lu [1] conducted an experimental program with small-scale API tanks subjected to internal deflagrations. The study examined tanks with continuous and discontinuous welding (stitch welding) along the roof-to-shell joint and found that stitch-welded tanks exhibited lower failure pressures and reduced shell distortion compared to fully welded tanks. The research revealed that the current guidelines provided by API 650 are inadequate for predicting the failure pressure of frangible roofs during internal deflagrations. The understanding of the frangible behavior of roof-to-shell joints, including activation pressure, variable ventilation area models, and turbulence effects, remains incomplete. Nevertheless, tanks with frangible roofs designed according to standard specifications have generally been successful in preventing failure at the bottom-to-shell joint. While the specifications have effectively addressed the failure mechanism, further comprehension of the phenomenon is still needed.

In line with this research, Hernandez [11] conducted a preliminary design of three small-scale API tanks, each employing distinct ventilation technologies. The first tank utilized a stitch weld pattern at the roof-to-shell joint. The second tank incorporated both a stitch weld pattern and a hinged opening on the roof, designed to open at low pressure levels, facilitating ventilation within the tank. Lastly, the third tank featured two massive venting panels mounted on the roof, offering ample ventilation to mitigate internal tank pressure and prevent explosions. These tanks were constructed and experimentally tested in a high-quality explosion test facility in China to study the response of fuel tanks subjected to internal deflagrations.

On the other hand, in recent years, research conducted by Li J. has focused on improving the prediction and understanding of internal and external pressures resulting from vented gas explosions through analytical and numerical methods, including Computational Fluid Dynamics (CFD) and simulations in the commercial software FLACS [12], along with experimental validation. Correlations have been developed to estimate peak overpressures in a faster and more accurate manner than NFPA standards [13–15], considering factors like

2

burning velocity, turbulence generation, and flame instability [16]. The effect of separation between explosion sources has been studied, establishing the relationship between tank separation and vented explosion pressure [17]. Additionally, accurate predictions of far-field overpressures for vented gas explosions are made, including the proposal of equations that provide a high level of accuracy in predicting the pressure-time history [18]. Furthermore, predictions have been made for both internal and external pressures in large enclosures and large cylindrical tanks, including the estimation of impulse generated by these vented gas explosions [19,20].

Based on the three designed tanks by Hernandez [11] and his experimental results, as well as considering the level of accuracy with which Li [16–20] models the fluid dynamics of the explosion in Hernandez's experimental tests, this research will focus on the numerical analysis and structural response of small-scale tanks subjected to internal deflagrations. The study will utilize the experimentally measured over pressures acting on the system to generate finite element models, allowing for the examination of the structural response of a FS tank under internal deflagrations based on the proposed ventilation technology. Particularly, experimental overpressure-time histories are used to model the answer of small-scale tanks on LS-DYNA [21–23]. Data given by the model is compared with the results of previous simulations, structural member calibrations were carried out to establish the response in some structural members during the explosions and an equation modeling the activation pressure of a tank with a frangible roof using a stitch weld pattern is presented.

In the first chapter, the experimental background that supports this research will be presented, where the detailed design of the tanks carried out by Hernandez [11] and their main characteristics will be explained. Additionally, the experimental setup used to conduct the tests of ventilated explosion will be described, and the results obtained from these experiments will be presented. In the second chapter, the finite modeling performed using LS-DYNA software will be explored, specifying the model's assumptions, and a comparison will be made between the results obtained experimentally and those generated by the simulation. Finally, the conclusions of this research will carefully consider the structural responses observed in each case, facilitating a comprehensive and cohesive analysis of the findings.

2. Field Blast Tests

2.1. General Design Assumptions

The tanks shown in Figure 1 were designed according to API standards for experimental gas explosion testing purposes. Each tank is 1.5 m in diameter and 1.0 m high, with a conical roof slope of 1/16. The primary focus of the study is the frangibility of the roof, which necessitates the incorporation of a massive foundation to counteract potential overturning resulting from the roof unbalanced ventilation. This is crucial as the roof ventilation generates a substantial overturning moment (recoil forces), which can be effectively compensated by a

heavy foundation. To ensure structural integrity, the shell thickness is verified under the assumption of a fully fuel-filled tank. However, the requirements for frangible roofs outlined in API 650 [2] and EN 14015:2004 [3] cannot be met due to the observation that frangible behavior is mainly evident in tanks with diameters larger than 12.5 meters. Additionally, a circular bottom plate is chosen rather than an annular bottom plate, due to the facility to be constructed and transported. Furthermore, this geometry provides a better stress distribution and higher confinement.
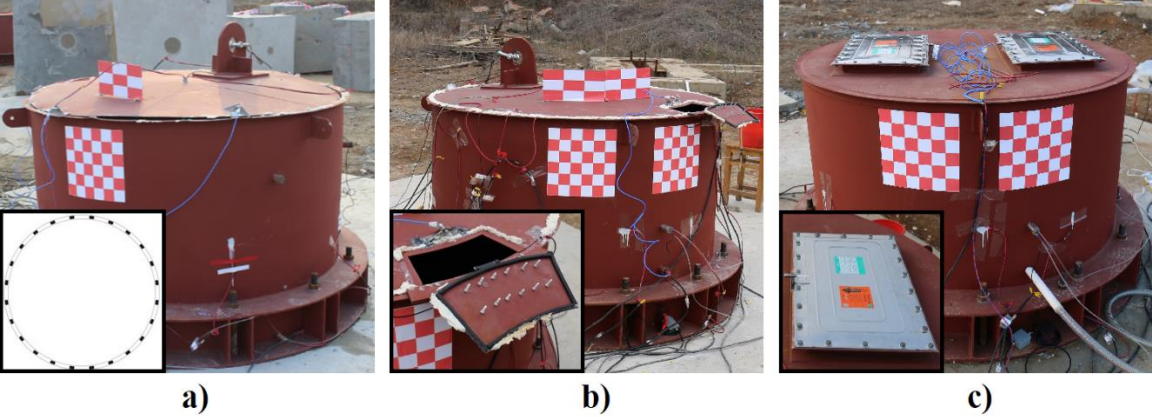
Figure 1: a) Type 1 Tank: Stitch-weld pattern b) Type 2 Tank: Hinge opening c) Type 3 Tank: Vent panels.

The structural calculation done by Hernandez [11] followed the American standard codes and used specific materials. To design the tank's main structure (including the shell, roof, ring plate reinforcement, base plate, skirt support, top plate, and gussets), ASTM A36 was used. Carbon structural steel ASTM A36 (F1554) was used for the anchoring bolts of 1 in diameter each. The foundations were designed using normal-weight Portland cement concrete that has a standard compressive strength of 3000 psi or higher. Steel bars of ASTM A706 Grade 60 was used for the concrete reinforcement and the selected weld electrode was E70 XX. Due to the unavailability of a geotechnical report on the soil conditions, a robust foundation was designed taking a conservative approach, particularly in the event of encountering weaker soil conditions.

2.2. Type 1 Tank: Stitch weld pattern

The Type 1 Tank employs a stitch-weld pattern, which involves 24 evenly spaced welds to connect the shell and the roof, with each weld measuring 35 mm in length (18% of the perimeter approx.) and 3 mm thick. This weld disposition strategically positions the failure near the connection weld or the shell, effectively imparting frangibility to the roof while facilitating ventilation inside the tank upon failure. This intentional design guarantees that failure occurs at a lower pressure level. This can be exemplified by employing the equations provided by API 650 [3], comparing the resultant force generated in a stitch weld pattern to that in a continuous weld. The resultant force in a continuous weld is over five times greater than in a stitch weld pattern (considering the Type 1 Tank's weld pattern), further emphasizing the effectiveness of the chosen design in ensuring controlled failure.

4

2.3. Type 2 Tank: Hinge opening

The Type 2 Tank shares similar assumptions with the Type 1 Tank, except for a couple of differences. Instead of 24 stitch-welds, the Type 2 Tank is equipped with 22 stitch-welds and incorporates a small vent opening specially designed to activate rapidly at a controlled pressure level, lower than that required for the roof activation. This design classifies the gas explosion as a partially confined explosion, as the small vent activates upon pressure build-up. The incorporation of this ventilation mechanism proves highly effective in mitigating the explosion, particularly for low and medium intensity explosions, thereby preventing structural failures. However, in cases where the activated vent's ventilation fails to fully mitigate the explosion, the pressure may continue to escalate, leading to roof failure. The hinge panel's activation plays an essential role, rapidly initiating ventilation and accelerating the failure of the frangible roof through global bending. This dynamic interaction ensures a faster activation of the frangible roof, providing precise control over the roof failure mechanism which propels it in the opposite direction of the hinge opening panel.

2.4. Type 3 Tank: Vent Panels

The Type 3 Tank features a continuous weld with a thickness of 5 mm and is equipped with two venting EGV panels [24] symmetrically positioned on the roof. These EGV panels are designed to activate rapidly at low opening pressure, but they are explicitly restricted from providing a massive ventilation surface during their activation phase. This controlled activation plays an important role in effectively mitigating the explosion by safely releasing pressure and preventing any sudden or uncontrolled failure in the tank.

2.5. Experimental Configuration

Figure 2 shows how the tank and the measurement system are arranged. All tanks have a circular bottom plate anchored to a reinforced concrete foundation to keep them stationary during gas explosions. High-strength bolts of 25.4 mm diameter were used, and PSB pressure sensors were mounted using hex nuts and rubber washers for equipment impermeability. High-speed video cameras (HSVC) with tracker panels were attached to the tank roof and shell. Bird sensors were installed on the roof to detect the moment when the roof was opened, and strain gauges were used both on the tank's shell and roof to measure the deformations experienced during the tests. Pressure transducers were set to measure peak pressures of 1000 kPa and were bolted onto the inner tank wall. Signals were logged on a 16-Bit A/D converter sampling at 50 kHz. Four isolation flange valves (0.75-inch diameter) were mounted on the shell for air discharge, gas inlet, and outlet. A polyethylene film was installed under the vent panels to prevent gas leakage during the gas filling process, and low-strength latex foam sealant was used to seal top roof holes and welding gaps, as shown in Figure 3. HSVCs were placed at 10 m from the tank, each with angles of 52.5 and 97.5 degrees (Figure 4), and with resolutions and shutter time of 2000-3000 fps and shutter time of 1/50, respectively. A Through-The-Lens (TTL) system was used to synchronize HSVCs with sensors. The inlet

flammable methane-air mixture was controlled by a Gas Flow Control System (GFCS) as shown in Figure 4, and a vent duct was used to release gas from the tank to maintain initial atmospheric pressure.
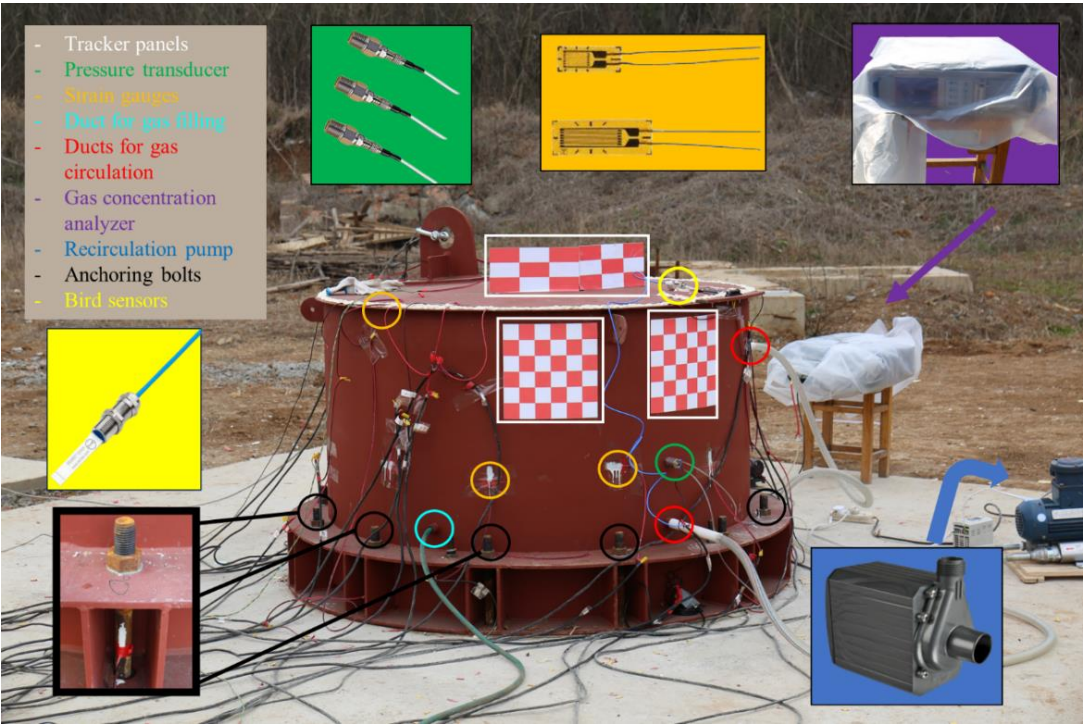

Figure 2: Setup of measure system.

In addition, a recirculation pump and an infrared methane analyzer were used to measure and control the gas–air concentration. Ionization probes and an electric spark plug were used as an ignition source located at the center of the tank (Figure 3). Q345B steel was employed to build the tanks, with a tensile strength ranging between 470 MPa and 630 MPa, and a yield strength of 345 MPa. The weld material adheres to the local Executive standard GB/T8110-2008. The tested properties of the weld material reveal a yield strength of 450 MPa and a tensile strength of 530 MPa.
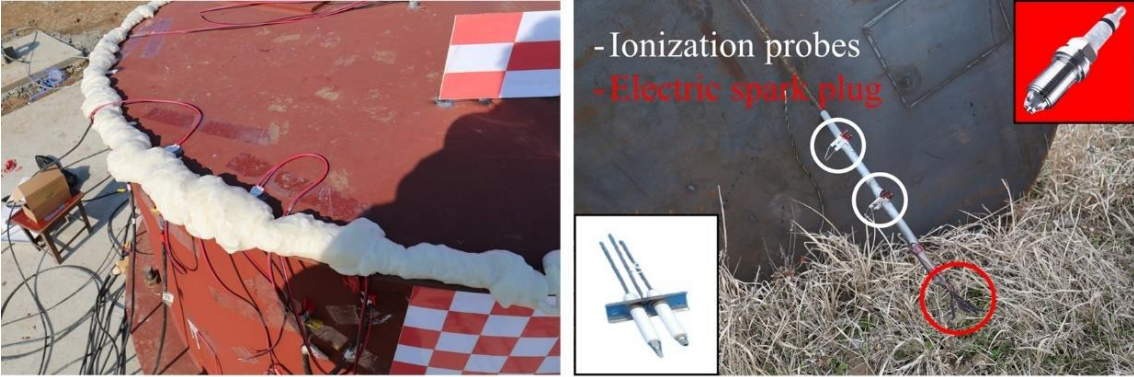
Figure 3: Latex foam sealant (left), ionization probes and electric spark plug (right)
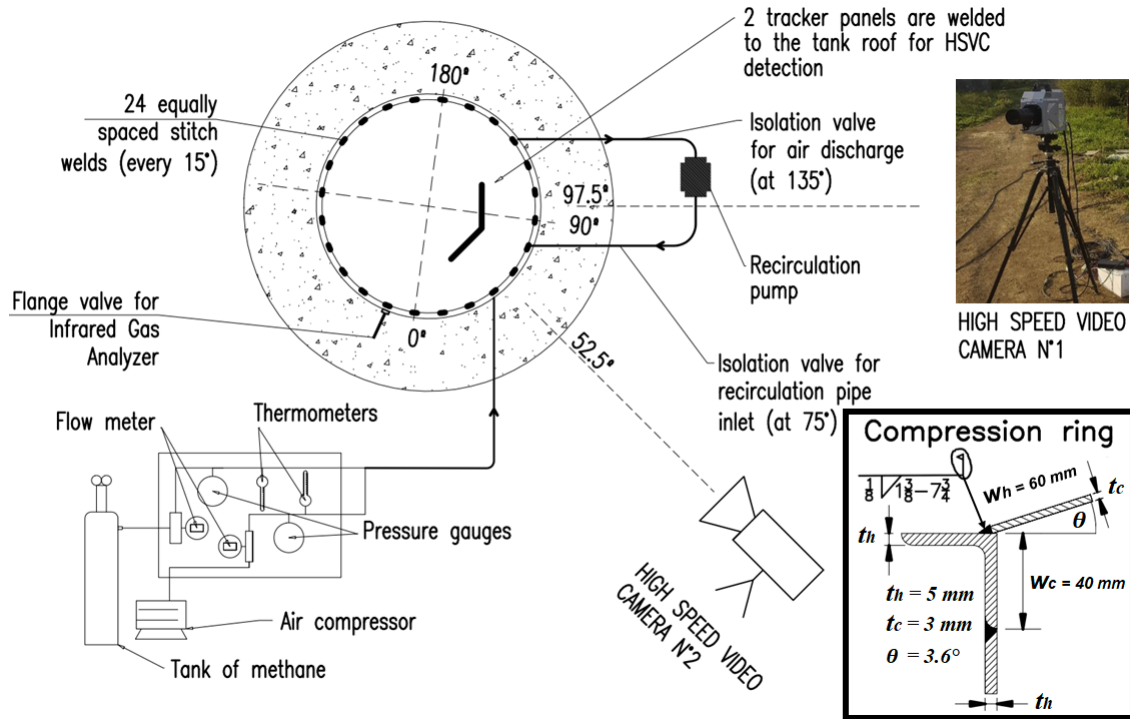
6

Figure 4: Experimental set-up on site and compression ring section.

2.6.   Experimental Results

Six field gas explosion tests were conducted, but only five of them were considered because the first one did not properly record the internal pressure. After the experiments, the shell and the anchoring system did not show perceptible damage and responded elastically. The mechanism of failure agreed with the predicted (stitch-welds failure). The plastic collapse of the compression ring and buckling of the roof or the shell were not observed. The stitch weld pattern, in the Type 1 tank, successfully provided a frangible roof.

Figure 5: Plasticization of the top ring (left), stitch weld failure during the experiments (right).

The activation pressure was properly predicted from previous numerical analysis [11] and overpressure was big enough to fully yield the 24 equally spaced welds or the roof material next to the welds (Figure 5), propelling the roof over 10 m away. Subsequently, three tests were conducted for the Type 2 tank. Particularly, test No. 2 and No. 3, which involved a methane-air concentration of 6.5%, resulted in the rapid and effective opening of the hinged

panel, providing ample ventilation to mitigate the internal pressure on its own, owing to the relatively low explosion pressure required for panel activation. However, in test No. 4, where a methane-air concentration of 9.5% was used, the hinge panel opened but led to roof failure thereafter. On the other hand, in test No. 5 for the Type 3 tank, both vent panels opened simultaneously, providing a significant vent area that effectively mitigated the effects of peak pressure and prevented tank failure. Internal overpressures are monitored at 500 mm and 750 mm in height. Since both graphics show different values, due to the calibration of the sensors employed, an average overpressure-time history is used for study purposes. Figure 6 shows a chronological sequence of the failures of each Tank during the tests.
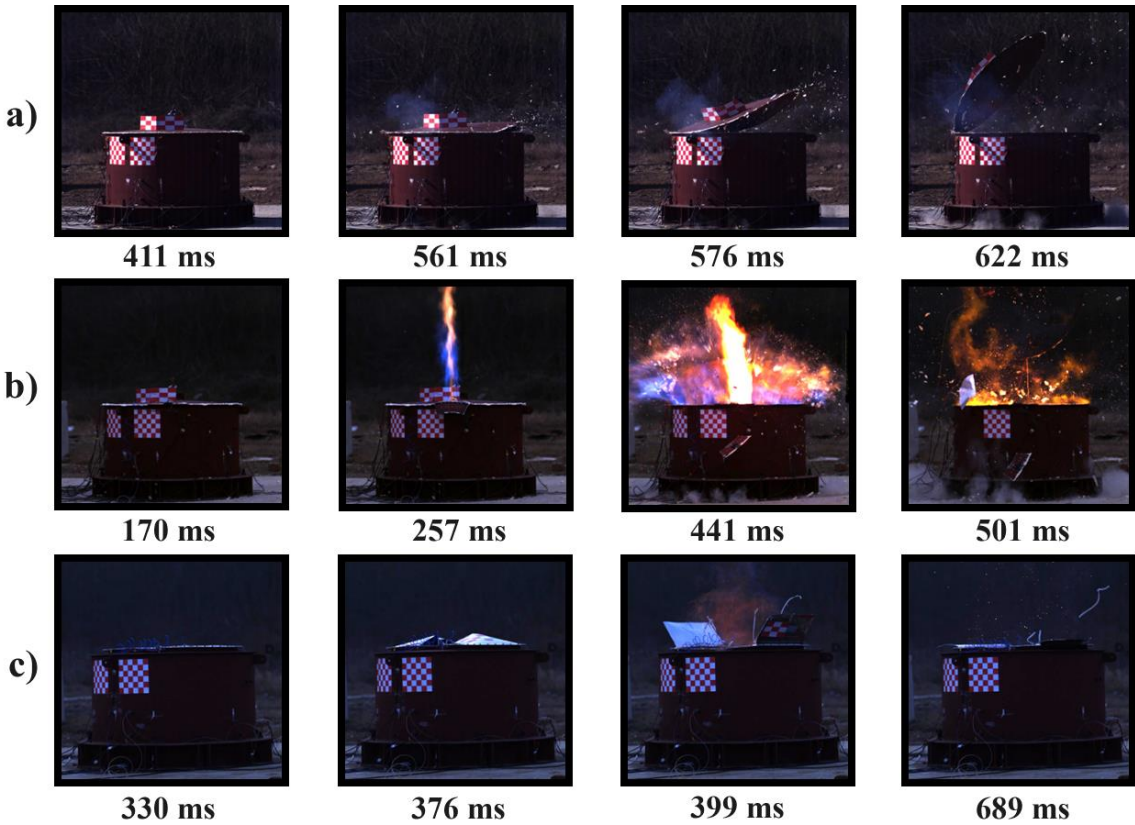

Figure 6: Potograph sequence related to a) Tank1, Test No.1, b) Tank 2, Test No.4, c) Tank 3, Test No.5

Table 1 shows a summary of the aforementioned results in addition to the overpressure time history graphics of each test, (meticulously adjusted to eliminate any inherent data noise), the most important pressure values on each experience (where P_{act} is the ventilation activation pressure, P_{roof} is the roof failure pressure and P_{max} is the maximal internal pressure during the experiment), and their respective occurrence times in milliseconds. It is possible to notice that the Type 1 tank has no vent activation pressure since it only considers a stitch weld in its design. Its roof failure pressure, 62.5 kPa, coincides with a maximal internal pressure at 554.0 ms. On the other hand, the Type 2 tank does not show roof failure pressure in tests number 2 and 3, due to the hinge panel, which provided enough ventilation to mitigate the explosion. The panel activations occur at 294 ms and 344 ms, reaching pressures of 8.5 kPa and 6.2 kPa
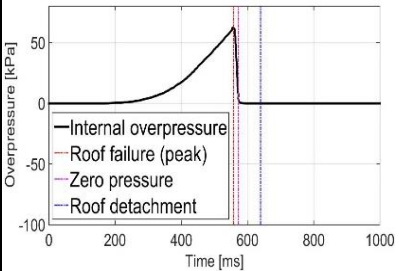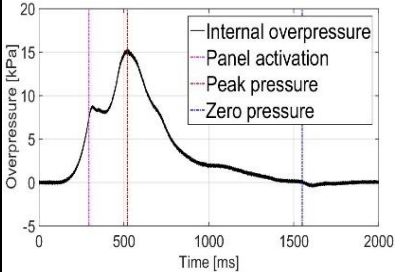
8
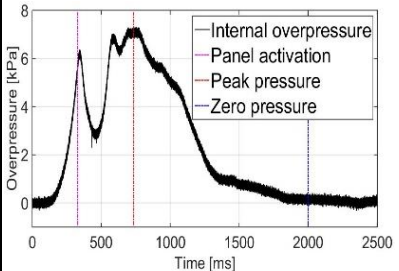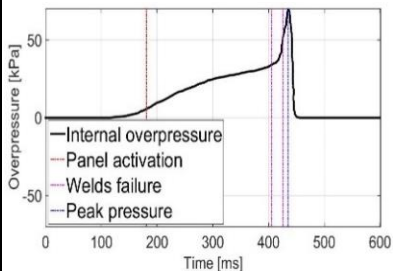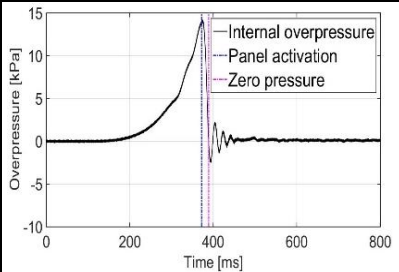
Test specifications	Venting mode	Pressure values (time)	Overpressure-time history
Test No. 1 Type 1 Tank 24 stitch welds 6.5 vol% methane-air		P_{act} [kPa] - P_{roof} [kPa] 62.5 (554.0 ms) P_{max} [kPa] 62.5 (554.0 ms)	
Test No. 2 Type 2 Tank: 22 stitch welds and a hinged vent panel 6.5 vol% methane-air		P_{act} [kPa] 8.5 (294.0 ms) P_{roof} [kPa] - P_{max} [kPa] 15.5 (514.8)	
Test No. 3 Type 2 Tank: 22 stitch welds and a hinged vent panel 6.5 vol% methane-air		P_{act} [kPa] 6.2 (344 ms) P_{roof} [kPa] - P_{max} [kPa] 7.1 (735 ms)	
Test No. 4 Type 2 Tank: 22 stitch welds and a hinged vent panel 9.5 vol% methane-air		P_{act} [kPa] 6.3 (181 ms) P_{roof} [kPa] 48.0 (425 ms) P_{max} [kPa] 70.0 (435 ms)	
Test No. 5 Type 3 Tank: Explosion vent panels on the roof 6.5 vol% methane-air		P_{act} [kPa] 14.2 (372 ms) P_{roof} [kPa] - P_{max} [kPa] 14.2 (372 ms)	

Table 1: Summary of the experimental results.

(for tests No. 2 and No. 3), followed by the maximal internal experimented pressure at 514.8 ms and 735 ms of 15.5 kPa and 7.1 kPa, respectively. Test No. 4 shows a similar panel activation pressure (6.3 kPa) to the previous test, at 181 ms, followed by the roof failure pressure (48.0 kPa) and the maximal pressure (70.0 kPa), at 425.0 ms and 435.0 ms, respectively. Furthermore, the Type 3 tank test does not suppose a roof failure pressure,

because vented panels provided a massive vent area able to release the overpressure inside the tank, experimenting with the maximal pressure and the vent activation pressure at 372 ms with a pressure value of 14.2 kPa.
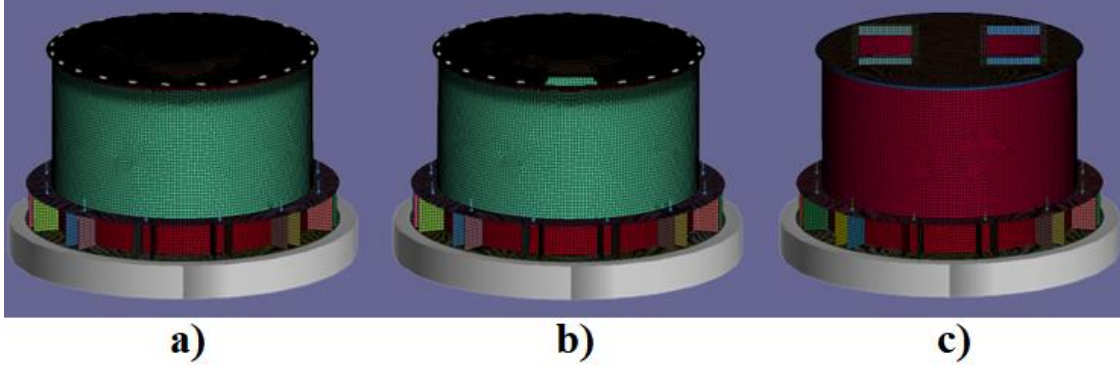
3. Numerical Simulations

Figure 7: Type 1 to 3 tank modelled in LS-DYNA. a) Type 1 Tank: Stitch-weld pattern b) Type 2 Tank: Hinge opening c) Type 3 Tank: Vent panels.

Finite Element simulations were conducted using evidence from the Field Blast Tests and leveraging previously developed models by Hernandez [13]. Figure 7 illustrates the 3D geometries of the three different tank types modeled in LS-DYNA. The primary focus of this investigation is to examine the frangible behavior of the proposed small-scale tanks, with the assumption that the failure mechanism is primarily influenced by the weld rather than the compression ring area. To simulate Type 1 and Type 2 Tanks, a stitch weld pattern is employed in the simulations (Type 3 Tank use a continuous weld). The objective is to achieve failure predominantly governed by a brittle failure of the stitch welds, while minimizing plastic strain experienced at the point of failure. For this purpose, the steel is modeled using the Simplified Johnson-Cook material model. The Johnson-Cook parameters for Q345B steel, along with Young's Modulus E_s, and Poisson's ratio v_s, are experimentally obtained and presented in Table 2 [25,26]. Self-weight of the structure is calculated from the specific weight of each material. Then, the total weight is $14.56 \, tonf$. The internal overpressures recorded during the field blast tests (Table 1) were applied to the model in order to simulate the corresponding overpressure-time history obtained experimentally.

$A\,[MPa]$	$B\,[MPa]$	N	C	$E_s\,[MPa]$	v_s
356	760	0.62	0.056	210000	0.26

Table 2: Q345B steel parameters for the Simplified Johnson-Cook model.

The maximal overturning moment expected is given by the recoil forces considering the assumption of Hernandez [13], and according to equations proposed by NFPA 68 [13] and EN 14994:2007 [27]. The static load on the structure caused by recoil forces is $F_R = 5.743 \, tonf$. Therefore, the maximal overturning moment experienced in the base of the shell and anchoring system is $M_R = 5.743 \, tonf * m$.

10

On the foundation side, a rigid wall assumption is made beneath the structure, and a surface-to-surface contact is established to connect the tank and the rigid foundation. This contact interface only allows for the transfer of compressive forces between the foundation and the tank's bottom plate. The anchor bolts are represented as springs designed to withstand only tensile forces. The stiffness of these springs is determined based on an assumed bolt length of 510 mm. The anchor bolts are modeled using a perfect elastic-plastic material model. For connecting the roof and the shell of the tanks, spot welds are employed. The mesh size is chosen to ensure that spot welds are evenly distributed at 5 mm intervals along the connection between the roof and the shell. Spot welds are represented by rigid beams that connect two nodal points, with the rotation and displacement of these points interconnected. It is assumed that the weld provides the same strength around the perimeter.

The pre-design conducted by Hernandez [11] took a cautious approach by assuming a peak pressure of 300 kPa. The simulation results indicate that the tank does not fail (i.e., it remains non-frangible) when a continuous weld is utilized. Moreover, the theoretical pressure failure values for each tank were determined based on the modeling performed in this pre-design. Upon comparing these theoretical values with the experimental data (presented inTable 1), it becomes evident that only the Type 1 Tank fails, even though it does not reach the expected theoretical pressure value (80 kPa). This observation suggests that the roof detachment of the tank cannot be solely attributed to the failure of each weld surrounding it. In the case of the Type 2 Tank, it fails during Test N°4 at a pressure higher than initially anticipated (27.9 kPa). Conversely, the Type 3 Tank activates its vent panels at a higher-pressure value than originally expected (10 kPa) during Test N°5.

Considering all these factors, the analysis employed the experimental overpressure-time data in conjunction with high-speed camera footage. This meticulous approach facilitated the precise manipulation of weld failure times experimented by Type 1 and 2 Type, thereby ensuring a faithful replication of roof failure dynamics during the LS-DYNA explosion simulation (Figure 8). Elevated weld strengths were deliberately applied to each spot weld, orchestrated to induce failure at the designated moments. Consequently, the simulation revealed the actual strength of each weld, which could then be juxtaposed against the presumed nominal threshold. The ensuing outcomes are detailed in the subsequent section. The results are presented below.
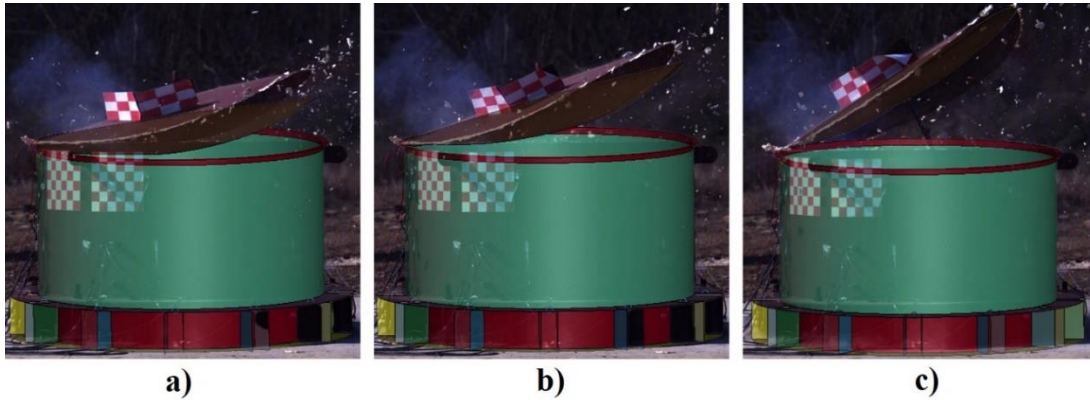
Figure 8: Superposition of experimental results captured by HSVC and simulation in LS-DYNA for Type 1 Tank at a) 572 ms b) 578 ms c) 592 ms

3.1. Type 1 Tanks' results

The Type 1 Tank model employs a stitch-weld pattern, which involves using 24 equally spaced welds to connect the shell and the roof. Each weld has a length of 35 mm and is created by eight consecutive and evenly spaced spot welds. Just as it occurred in the experiment, due to the high concentration of stresses near the welds (Figure 9a), the failure occurs at 554 ms, causing a sequential failure of the roof. The ventilation occurring within the tank, due to the roof opening, can be observed by examining the Von Mises stress before, during and after the roof failure, as depicted in Figure 9.
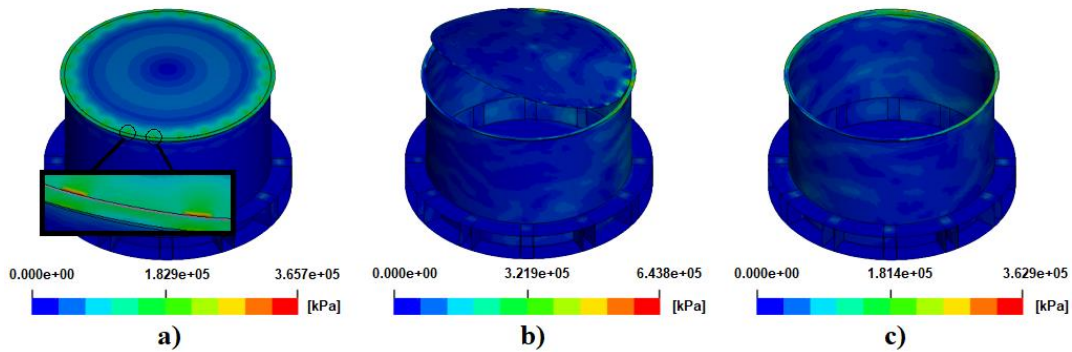

Figure 9: Von Mises stress experimented at a) 553 ms b) 580 ms c) 647 ms

The outcomes of the model's analysis demonstrate that the weld strengths are situated within the 1.75 kN range, equating to approximately 35% of the nominal weld strength. Figure 10 provides a visual representation of the evolution of effective plastic strain during the initiation of roof failure. Notably, the most prominent instances of effective plastic deformation are observed in close proximity to the stitch welds. Just before the moment of failure (at 553 ms), it becomes evident that the plastic strain exhibits uniformity adjacent to each weld, with an approximate value of 1.4%. However, post-failure, a significant transformation occurs, with the roof experiencing considerably elevated levels of plastic strain. These magnitudes, ranging between 6% and 15%, instigate the yielding of the roof material within the structure. Furthermore, the roof plastic strain levels rise substantially beyond the yield point, indicating

12

the roof material's inability to withstand the imposed load. In fact, the outcomes of the model's analysis demonstrate that the weld strengths are situated within the 1.75 kN range, which is equivalent to only 35% of the nominal weld strength. Although the welds do not achieve their maximum strength potential before giving way, they play a crucial role in mitigating further escalation of plastic deformation within the structure. Ultimately, this sequence of events leads to failure, primarily attributed to the intrinsic properties of the roof material. Consequently, the discernible weld pattern exerts a significant influence on the frangible behavior of the structure.
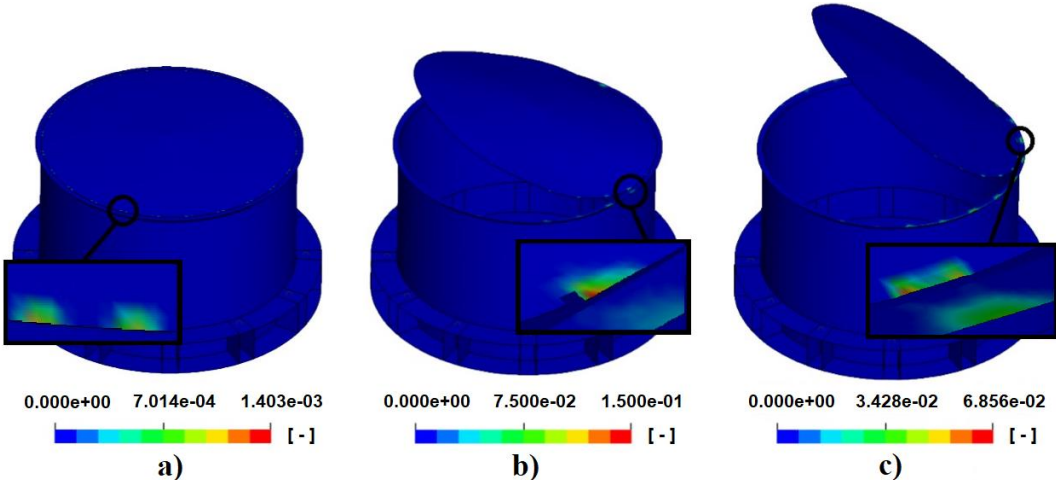

Figure 10: Effective plastic strain experimented at a) 553 ms b) 582 ms c) 591 ms

On the other hand, when simulating this tank considering a continuous weld in the roof-to-shell junction (involving the whole perimeter with stitch welds), alongside the application of the same overpressure curve, the point of structural failure is not reached. However, upon amplifying the experimental pressure data by a factor of four (equivalent to a maximum pressure of 250 kPa), the tank does not fail but it exhibits significant levels of plastic deformation along the compression ring, resulting in enduring deformations within the structure. This observation implies that the structural failure could originate in the compression ring under substantial overpressure conditions within the tank. Alternatively, failure might manifest in other structural components, such as the tank shell or its foundation. This circumstance contradicts the underlying design principle of an inherently frangible nature for the roof. Such a collapse would lead to irreparable damage to the structure. Considering the magnitude of attainable pressures, it could lead to catastrophic consequences for the tank and its surrounding area.

Despite these observations, the equations introduced by API 650, which aim to compute the ultimate resistance for the compression ring, yield values considerably lower than those capable of causing failure in this tank (approximately 22 kPa). This disparity arises due to two reasons. First, the effective lengths that API 650 considers in the calculation of the compression ring's strength remain constant as both the shell and roof of the tank start undergoing plastic deformations. This leads to an increase in the effective lengths within the

section and, consequently, a significant rise in the tank's strength. Numeric expressions provided by other authors (such as the Rotter [28] equation) are more suitable for predicting the roof activation pressure (about 69 kPa for the case of Type 1 Tank). However, this equation does not account for the assumption that the tank's shell and roof will undergo large deformations, thereby underestimating the level of strength achieved by the compression ring. Second, the presumption in the API equations that the structure behaves in a static manner. However, reality differs as tanks, due to the rapid load application during an explosion, exhibit dynamic behavior. Consequently, when conducting a dynamic simulation of a tank featuring continuous welding, the achieved resistance level significantly surpasses the forecasts of the API equations. Taking this into account, the failure of the compression ring is applicable only when pseudo-static or operational pressures are taken into consideration for a storage tank. It is not suited for designing this structure to withstand explosive loads, given the dynamic attributes of the explosions. Thus, API equations are inadequate for modeling explosive events.

However, when employing stitch weld pattern, the system's behavior becomes pseudo static. This characteristic arises because the natural frequency of the Type 1 Tank is approximately 145 Hz, while an analysis of the Fourier transform applied to the experimental overpressure record reveals pulse frequencies around 60 Hz. Consequently, the dynamic amplification factor in the structural response is approximately 0.4, yielding a pseudo static response, regardless of the level of inherent damping in the structure. Therefore, it is possible to determine the activation pressure of the tank's roof using a stitch weld pattern with the following equation:

$$P_r = \frac{F_u * t_w * n_{sw} * L_{sw} * \sin(\xi\theta)}{A_r} \tag{1}$$

Where F_u is the ultimate tensile strength of the roof material, t_w is the thickness of each stitch weld, A_r is the roof area, n_{sw} is the number of stitch welds around the perimeter of the tank, L_{sw} is the stitch weld's length, θ is the roof slope expressed in degrees and ξ is a roof angle correction factor (between 1.0 and 2.0).

3.2. Type 2 Tanks' results

The Type 2 Tank incorporates a small vent opening specially designed to activate rapidly at a controlled pressure level, lower than that required for the roof activation. Additionally, it is equipped with 22 stitch-welds. Each weld has a length of 35 mm and is created by eight consecutive and evenly spaced spot welds. Tests 2 and 3 simulations demonstrate the efficacy of the hinge opening as a ventilation mechanism to swiftly mitigate internal pressure within the tank. This ingenious design not only averts potential explosions but also maintains structural integrity during the explosion. The figure illustrates the stress distribution within the structure, with the highest forces concentrated near the welds on each side of the gate.

Furthermore, it can be observed that, following the activation of the gate, deformations remain within a linear range. This outcome proves particularly invaluable for swift containment of minor explosions.
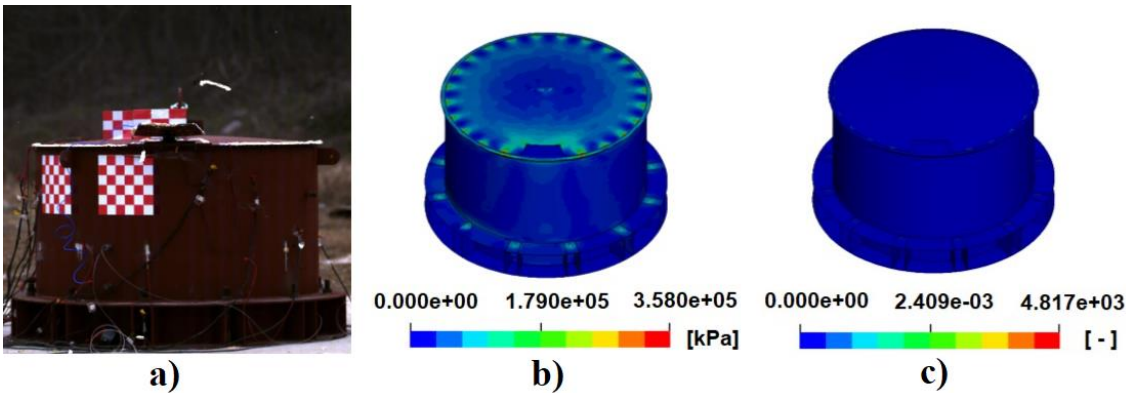

Figure 11: a) Type 2 Tank during the field blast test (at 660 ms) b) Von Mises stress at 660 ms c) Effective plastic strain at 660 ms

Otherwise, if the vent's activated ventilation fails to adequately mitigate the explosion, it is anticipated that the pressure will continue to escalate, resulting in the failure of the roof (as it happened during Test 4). The model replicates the same roof failure as observed in the experiment, with the failure initiating at 435 ms. Remarkably, the absence of the two welds on the hinged opening's covered surface becomes evident as a pivotal factor. This absence triggers the initial weld failures in the adjacent regions of the opening (Figure 12a). The vent's prompt activation channels pressure concentration to this specific area, subsequently inducing the sequential failure on the roof. The consequence is the ejection of the roof in a trajectory diametrically opposed to the opening's location, as illustrated in Figure 12.
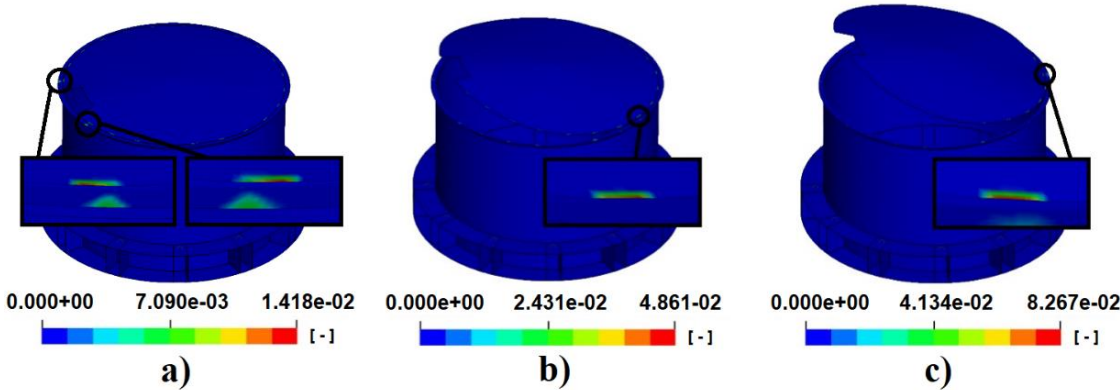
Figure 12: Effective plastic strain experimented at a) 425 ms b) 445 ms c) 452 ms

The resistance observed by the welds is approximately 1.1 kN, which represents 24% of the nominal strength. Meanwhile, the levels of plastic deformation reached in this tank range from 4% to 9%. This suggests that the stress concentration in the welds near the tank's opening leads to their failure, causing a sequential failure in the material connecting the roof to the other welds (similar to what happens in Type 1 Tank).

15

3.3.   Type 3 Tanks' results

The roof plate of Type 3 Tank is welded by a continuous seal weld of 5 mm around the entire perimeter. As evidenced by the experiment, the simulation demonstrates how the substantial ventilation panels adeptly discharge internal pressures from the tank, thereby effectively curbing the potential for explosion and ensuring the structural integrity remains unscathed. Notably, post-explosion assessments reveal the presence of null plastic deformations within the tank (Figure 13c). Additionally, after the activation of the ventilation panels, the gas concentration predominantly congregates atop the structure's roof. This phenomenon arises from the ventilation mechanism's strategic intent to alleviate the incumbent pressures concentrated at the tank's zenith (as depicted in Figure 13). While the stress levels register as modest, their inclusion in the design considerations holds paramount significance.
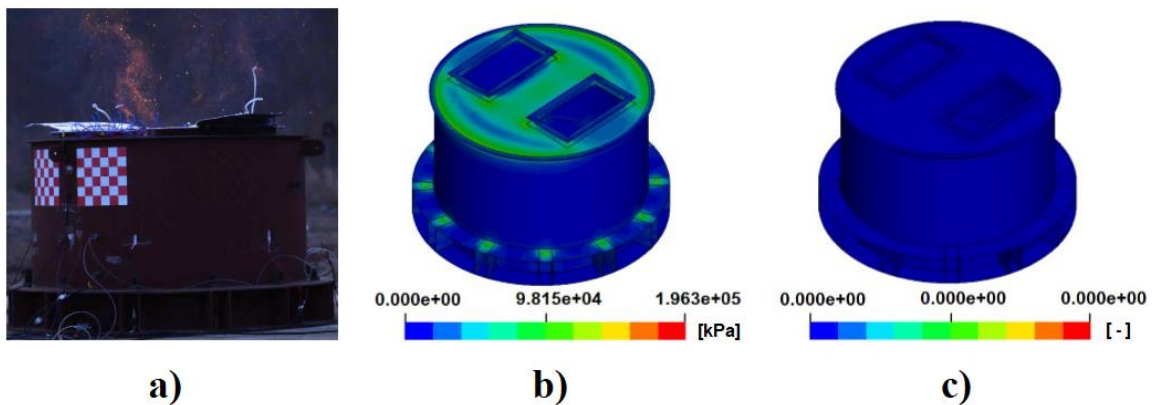

Figure 13: a) Type 3 Tank during the field blast test (at 468 ms) b) Von Mises stress, tank 3 at 468 ms c) Effective plastic strain during the simulation

4. Conclusions

A comparison was conducted between the experimental evidence from tests on fuel tanks subjected to internal deflagration. These tests involved three types of tanks with different ventilation systems on their roofs. Finite element modeling of the tanks, including their respective ventilation technologies, was used for this purpose, and their responses were simulated, considering the experimentally obtained overpressures, using the LS-DYNA software. Additionally, the failure sequence was replicated in the welds along the perimeter of Type 1 and Type 2 Tanks. This allowed for obtaining the experimental strengths of each weld in each test, which were compared to theoretical values, yielding reasonable results. However, considering that the failure in the spot-weld joint within LS-DYNA can be attributed to issues in both the weld material and the material to which it is joined, in this case, the roof material. By observing the levels of plastic deformation attained in the vicinity of the welds as per the simulation results and considering the low percentage of performance experienced by the welds (35% and 24% respectively), the conclusion is drawn that the root of the problem lies in the failure of the roof material in the case of tank 1. Conversely, in the

16

case of tank number 2, the welds adjacent to the opening exhibit failure, subsequently triggering the failure of the roof material in proximity to these perimeter welds.

The stitch-weld pattern used in these tests successfully achieved a frangible roof behavior for the small-scale tanks playing a vital role in the concentration of stresses around it, leading to the opening failure of the roof in the structure. Consequently, this technology has the potential to be applied to small-scale tanks, enabling the implementation of a frangible roof that surpasses the limitations imposed by the API 650 standard, typically applicable to tanks with diameters exceeding 12.5 meters. Furthermore, stitch welds can be employed to lower the activation pressure of larger tanks, provided that the design ensures the roof can withstand operational internal overpressures. Additionally, this failure is not considered within the API 650 standard, which only considers failure through the compression ring in a tank. The equations by API 650 yield lower ultimate resistance values for the compression ring, unsuited for explosive load scenarios. The discrepancy arises because API equations assume scenarios of static loading on the structure, whereas an explosion is inherently a dynamic phenomenon. Furthermore, these equations do not consider the large deformations that the roof of a tank experiences when subjected to high levels of pressure within the structure. Therefore, API equations are insufficient for modeling explosive events. Consequently, this research proposes an equation to determine the roof's opening pressure in a FS tank that features a stitch weld pattern at the roof-to-shell junction of the structure.

The venting technology featured by Type 1 Tank exhibits a brittle failure in the stitch-weld pattern that connects the roof to the shell at low pressure levels. This failure allows for rapid ventilation within the tank, mitigating high pressure levels and preventing an uncontrolled explosion in the structure. However, this failure mode has a disadvantage: eventually, the roof could yield to pressure increases inside the tank, which are common during normal operations of a FS tank due to the filling and emptying cycle. This limitation can be overcome by using stronger welds or reducing the spacing between weld discontinuities along the joint. On the other hand, the advantage of only the weld failing is that the tank's integrity is not compromised during the explosion. This means that the roof can be repaired by welding, allowing the tank to return to proper functioning.

Type 2 Tank has stitch-welds and a hinge opening in the roof, which provides a ventilation area when activated. This ventilation mechanism is convenient as it can control excessive pressure during small explosions, as observed in tests number 2 and 3. The hinge opening can be closed again after use, either through welding or with the use of special adhesive, which will determine its activation pressure in future scenarios. In the case of experiencing higher levels of pressure, the hinge opening is activated, however, it is unable to provide sufficient ventilation to mitigate the explosion. As a result, the roof of the structure fails in the opposite direction to where the hinge opening is located (test number 4). This occurs because the stresses are concentrated around the opening, causing the roof material to progressively fail (due to stress concentration around the stitch welds) in the opposite

direction, what is convenient from a safety standpoint since, on one hand, this technology can mitigate small explosions, while also controlling and establishing a safe zone where the tank's roof can fall once the explosion occurs. In the future, further research can be conducted on the number and placement of such hinged openings that the tank's roof could have, and even evaluate different activation pressures for each one. This would allow for the design of a gate system on the roof that would open consecutively based on the pressure level experienced by the tank or further gate system technologies.

Finally, Type 3 Tank's technology provides a secure ventilation mechanism to the structure, ensuring its opening at a given pressure level. The vents accounted for 20.9% of the tank's cross-sectional area, providing sufficient ventilation to regulate internal pressure and reduce peak pressure to match the panel activation pressure. Moreover, the symmetrical configuration of the panels on the roof did not generate an overturning moment. The vent panels technology proves to be highly effective and straightforward in providing controlled ventilation. It prevents panels from being forcefully propelled away from the tank as they remain attached to the structure, thereby preventing collisions with neighboring structures. However, this technology necessitates multiple vent panels to achieve a vent area of 10-20% of the roof in real-scale tanks. Additionally, the supporting structure (whether the roof or the shell) must be adequately reinforced since openings can significantly weaken the roof strength. This technology can be useful in existing tanks with large roofs that need to enhance their ventilation system in the event of pressures significantly higher than operational ones.

5. Bibliography

[1]   Swenson D, Fenton D, Lu Z, Ghori A, Baalman J. Evaluation of design criteria for storage tanks with frangible roof joints. Weld Res Counc Bull 1996:1–71.

[2]   API-650. Welded Steel Tanks for Oil Storage, 11th Edition. Am Pet Inst 2007.

[3]   British Standards Institution., European Committee for Standardization. EN14015:2004 - Specification for the design and manufacture of site built, vertical, cylindrical, flat-bottomed, above ground, welded, steel tanks for the storage of liquids at ambient temperature and above. 2004.

[4]   Swenson, D; Fenton, D; Lu, Z.; Ghori A ;Baalma. J, Swenson D, Fenton D, Lu Z, Ghori A, Baalman J. Evaluation of Design Criteria for Storage Tanks With Frangible Roof Joints. 1996.

[5]   API-2000. Venting Atmospheric and Low-Pressure Storage Tanks. Am Pet Inst 1998.

[6]   Chang JI, Lin CC. A study of storage tank accidents. J Loss Prev Process Ind 2006;19:51–9. https://doi.org/10.1016/j.jlp.2005.05.015.

[7]   Marmo L, Piccinini N, Russo G, Russo P, L. M. Multiple tank explosion of pomace oil reservoirs. 2010.

[8]   Hailwood M, Gawlowski M, Schalau B, Schönbucher A. Conclusions drawn from the Buncefield and Naples incidents regarding the utilization of consequence models. Chem Eng Technol 2009;32:207–31. https://doi.org/10.1002/ceat.200800595.

[9]   Taveau J. Explosion of fixed roof atmospheric storage tanks, Part 1: Background and review of case histories. Process Saf Prog 2011;30:381–92. https://doi.org/10.1002/prs.10459.

[10]   EEMUA. Frangible Roof Joints for Fixed Roof Storage Tanks: Guide for designers and users. Eng Equip Mater Users' Assoc 2008.

[11]   Hernandez F. Explosive Protection of Storage Chambers through Frangible Structural Elements. SAGE Publications Inc., 2016.

[12]   GexCon AS. FLACS v9.1 User's Manual 2011.

[13]   NFPA. NFPA 68 - Standard on Explosion Protection by Deflagration Venting 2007 Edition. Natl Fire Prot Assoc 2007.

[14]   NFPA. NFPA 68 - Standard on Explosion Protection by Deflagration Venting 2013 Edition. Natl Fire Prot Assoc 2013.

[15]   NFPA 68. Guide for Venting of Deflagrations. Natl Fire Prot Assoc 2002.

[16]   Li J, Hernandez F, Hao H, Fang Q, Xiang H, Li Z, et al. Vented Methane-air Explosion

Overpressure Calculation—A simplified approach based on CFD. Process Saf Environ Prot 2017;109:489–508. https://doi.org/10.1016/j.psep.2017.04.025.

[17] Li J, Hao H, Shi Y, Fang Q, Li Z, Chen L. Experimental and computational Fluid Dynamics study of separation gap effect on gas explosion mitigation for methane storage tanks. J Loss Prev Process Ind 2018;55:359–80. https://doi.org/10.1016/j.jlp.2018.07.008.

[18] Li J, Hao H. Far-field pressure prediction of a vented gas explosion from storage tanks by using new CFD simulation guidance. Process Saf Environ Prot 2018;119:360–78. https://doi.org/10.1016/j.psep.2018.08.004.

[19] Li J, Hao H. Internal and external pressure prediction of vented gas explosion in large rooms by using analytical and CFD methods. J Loss Prev Process Ind 2017;49:367–81. https://doi.org/10.1016/j.jlp.2017.08.002.

[20] Li J, Hao H. Numerical and analytical prediction of pressure and impulse from vented gas explosion in large cylindrical tanks. Process Saf Environ Prot 2019;127:226–44. https://doi.org/10.1016/j.psep.2019.05.019.

[21] LSTC. LS-DYNA Keyword User's Manual - Volume I. 2017.

[22] LSTC. LS-DYNA Keyword User's Manual - Volume II - Material Models. 2017.

[23] LSTC. LS-DYNA Keyword User's Manual - Volume III - Multi-Physics Solvers. 2017.

[24] REMBE. EXPLOSION SAFETY, 2015.

[25] Seidt JD, Gilat A, Klein JA, Leach JR. High strain rate, high temperature constitutive and failure models for EOD impact scenarios. Proc. SEM Annu. Conf. Expo. Exp. Appl. Mech. 2007, vol. 1, 2007, p. 160–74.

[26] Li W, Qian LX, Feng GP, Li HM. The dynamic response of cylindrical shell and square plate with pre-formed holes under blast loading. J Phys Conf Ser 2020;1507. https://doi.org/10.1088/1742-6596/1507/3/032004.

[27] European Committee for Standardization. EN 14994:2007 - Gas explosion venting protective systems. Eur Comm Stand 2007;3.

[28] Rotter J.M. Buckling and plastic collapse of ring stiffeners at cone/cylinder junctions. Proc, Int Colloq Stab Plate Shell Struct, Gent, Belgium n.d.